LETTERS
PUBLISHED ONLINE: 29 JUNE 2014 | DOI: 10.1038/NNANO.2014.125
nature nanotechnology

Probing ultrafast spin dynamics with optical pump–probe scanning tunnelling microscopy

Shoji Yoshida[1], Yuta Aizawa[1], Zi-han Wang[1], Ryuji Oshima[2], Yutaka Mera[3], Eiji Matsuyama[1], Haruhiro Oigawa[1], Osamu Takeuchi[1] and Hidemi Shigekawa[1]*

Studies of spin dynamics in low-dimensional systems are important from both fundamental and practical points of view[1,2]. Spin-polarized scanning tunnelling microscopy allows localized spin dynamics to be characterized and plays important roles in nanoscale science and technology[3–5]. However, nanoscale analysis of the ultrafast dynamics of itinerant magnetism, as well as its localized characteristics, should be pursued to advance further the investigation of quantum dynamics in functional structures of small systems. Here, we demonstrate the optical pump–probe scanning tunnelling microscopy technique, which enables the nanoscale probing of spin dynamics with the temporal resolution corresponding, in principle, to the optical pulse width. Spins are optically oriented using circularly polarized light, and their dynamics are probed by scanning tunnelling microscopy based on the optical pump–probe method. Spin relaxation in a single quantum well with a width of 6 nm was observed with a spatial resolution of ∼1 nm. In addition to spin relaxation dynamics, spin precession, which provides an estimation of the Landé *g* factor, was observed successfully.

In nanoscale science and technology, the addition of high temporal resolution to scanning probe microscopy (SPM) has attracted considerable attention since its invention[4–9]. An approach to achieving such microscopy is to combine the techniques of quantum optics with SPM[9–15], and even single-atomic-level analysis has been realized by laser-combined scanning tunnelling microscopy (STM) based on the optical pump–probe (OPP) method[15]. As spin dynamics have been studied extensively by quantum optical methods and the interaction between spins and optics is a major subject in science and technology[2,16], to combine SPM with optical techniques is expected to be highly advantageous. Although studies that have employed optical SPM showed its high potential for characterizing quantum dynamics in small organized structures, the observation of ultrafast spin dynamics by optical SPM has not yet been achieved.

Here we present an STM technique realized by the development of a new modulation method with circularly polarized (CP) light that enables the nanoscale probing of spin dynamics with temporal resolution corresponding to the optical pulse width in principle (see Methods). Its performance is demonstrated by three major examples: (1) the temperature dependence of the relaxation of optically oriented spins in GaAs, which shows the basic spin interaction mechanisms; (2) the independent probing of spin dynamics in single GaAs/AlGaAs quantum wells with lifetimes dependent on confinement energy; (3) the quantum beat of spin precession, which provides the Landé *g* factor, a fundamental value in spin science and technology.

Figure 1a shows a schematic illustration of the OPP-STM technique we have developed. In OPP-STM for spin detection, the sample surface below the STM tip is excited by a train of CP pulse pairs and the change in tunnelling current is measured as a function of delay time[13]. As shown in Fig. 2a for GaAs, when the photon energy of CP light is adjusted to excite only the upper bands consisting of the heavy-hole and light-hole bands, the spin polarization becomes 50% (ref. 2). When the circular polarizations of pump and probe pulses are the same, namely, left-handed (L-) or right-handed (R-) rotation, we call this co-circularly polarized (co-CP) excitation. However, when they are different, we call it counter-circularly polarized (counter-CP) excitation. If co-CP or counter-CP excitation is used for the OPP method, the relaxation of spin orientation can be probed as a function of delay time because of absorption bleaching. Namely, if up (down) spins remain in the excited states, the excitation of up (down) spins is suppressed. Therefore, as shown in Fig. 1d, the number of electrons excited by the probe pulse, $n_{ex}^{co}(t_d)$ ($n_{ex}^{count}(t_d)$), increases (decreases) with delay time t_d for co-CP (counter-CP) excitation depending on the relaxation of the spin direction oriented by the pump pulse[17], which is reflected in the tunnelling current $I_S(t_d)$ (refs 13,14). Accordingly, with the new modulation method we have developed, the difference between the signals measured by the two excitation modes, ($\Delta I_S(t_d) = I_S^{count}(t_d) - I_S^{co}(t_d)$), can be obtained as a spin-related spectrum (see Methods).

First, the modulation system we have developed was evaluated by measuring the spin dynamics in GaAs (undoped) using the optical pump–probe reflectivity (OPPR) method and OPP-STM. In our OPPR measurement, a GaAs(100) sample was illuminated by optical pulse trains in air, as shown in Fig. 2b. The results are shown in Fig. 2c, and two components with decay constants of 0.49 ± 0.02 ps and 5.3 ± 0.8 ps were observed. Second, excitation by the pump and probe pulses with the combination of CP and linearly polarized (LP) light (CP + CP or CP + LP) was used to confirm that the signal was spin related: when the CP + LP combination was used, the signal disappeared, as expected. The relaxation lifetimes, which are twice those of the decay constants[17], are consistent with those for electron spins previously observed. The fast and slow components are attributed to the cooling of the excited electrons[18] and subsequent relaxation of the optically oriented spins in the conduction band[19,20] (relaxation of hole spins is much faster[2]).

Figure 2d shows a typical spectrum obtained by OPP-STM for the same GaAs sample using the new modulation technique. The GaAs(110) surface was prepared by cleavage in a vacuum (5×10^{-8} Pa, Omicron VT-STM). A chemically etched W tip was used. The photoexcitation was carried out at an angle of about 70° from the normal to the surface. The decay of spin orientation consists of two components with decay constants of 0.51 ± 0.01 ps and 5.8 ± 0.8 ps, which is in good agreement with the results obtained

[1]Faculty of Pure and Applied Sciences, University of Tsukuba, Tsukuba 305-8571, Japan, [2]Advanced Industrial Science and Technology, Tsukuba 305-8568, Japan, [3]Shiga University of Medical Science, Otsu, 520-2192, Japan. *e-mail: hidemi@ims.tsukuba.ac.jp

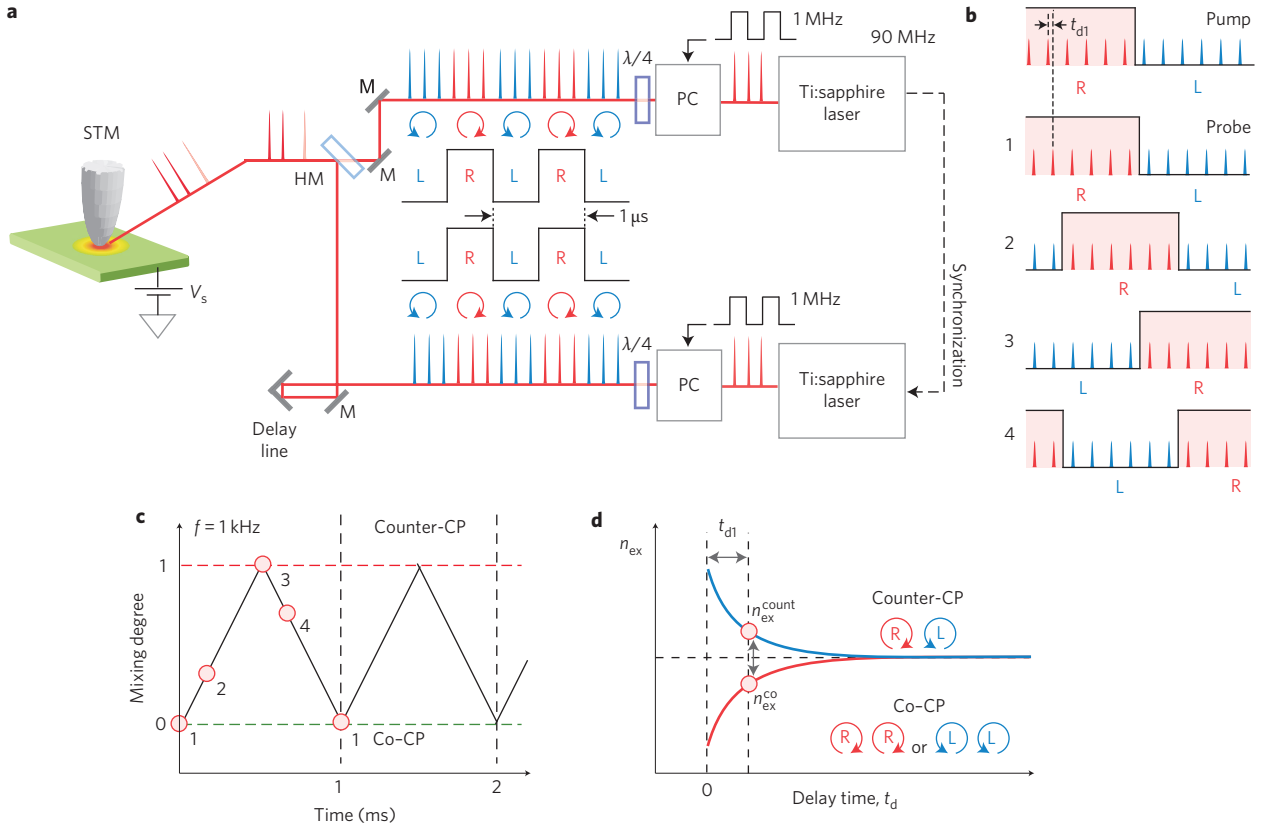

Figure 1 | OPP-STM used for spin detection. a, Schematic illustration of the OPP-STM technique. Two titanium:sapphire lasers (0.75 W and 0.7 W, 90 MHz, duration ~130 fs) were used with a Synchrolock system to produce pump and probe excitation. L (blue pulses) and R (red pulses) denote circular polarizations with L- and R-rotation, respectively. V_s is the bias voltage. PC is a Pockels cell. M and HM are a mirror and half-mirror, respectively. $\lambda/4$ is a quarter-wave plate. The red spot below the STM tip represents the photoexcited area. **b**, Modulation of circular polarizations of pump and probe pulses. t_{d1} is the delay time between the pump and probe pulses. The square wave indicates the times when the circular polarization is switched. **c**, Mixing degree of circular polarizations of pump and probe pulses: co-CP (0, green dashed line) and counter-CP (1, red dashed line) excitation at frequency $f = 1$ kHz. Points 1 to 4 correspond to the states in **b**. **d**, Spin-detection signal that can be measured by the two excitation modes of counter-CP excitation (blue line) and co-CP excitation (red line). n_{ex}, $n_{ex}^{count}(t_d)$ and $n_{ex}^{co}(t_d)$ indicate the number of excited electrons and the numbers excited by the two excitation modes, respectively. Using the new modulation method, $\Delta n_{ex}(t_d) = \Delta n_{ex}^{count}(t_d) - \Delta n_{ex}^{co}(t_d)$, indicated by the vertical grey arrow, can be measured.

by the OPPR method shown in Fig. 2c. The slower components are considered hereinafter.

This is the first-ever time-resolved STM observation of optically oriented spin dynamics in the picosecond range. A new method of microscopy, which enables the observation of ultrafast spin dynamics, has been realized successfully. To show the potential of this microscopy, we carried out three fundamental experiments, described as follows.

First, we measured the temperature dependence of the spin dynamics in GaAs. According to a theoretical study, the temperature (T) dependence of spin-orientation lifetime (τ_s) in non-centrosymmetric semiconductors basically follows the relationship $\tau_s \approx T^{-3}$ (Dyakonov–Perel mechanism)[2,21], in which spin rotates during collisions with impurities because of the spin-orbit splitting of the conduction band. In the case of p-type semiconductors, however, the spin relaxation of non-equilibrium electrons caused by the exchange interaction between the electron and hole spins produces the relationship $\tau_s \approx T^{-0.5}$ at low temperatures (Bir–Aronov–Pikus mechanism)[2,21].

A cleaved p-type GaAs(110) surface (Zn-doped, 5.0×10^{16} cm^{-3}) was used as the sample. Figure 3a,b shows the temperature-dependent spectra obtained by OPP-STM and their magnifications, respectively. The lifetime increased with decreasing temperature, which is summarized in Fig. 3c. The lifetime satisfies $\tau_s \approx T^{-3}$ at high temperatures and tends to saturate at low temperatures owing to the effect of the Bir–Aronov–Pikus mechanism, as expected, which indicates that OPP-STM works well.

Second, we carried out measurements on GaAs/AlGaAs quantum wells, as schematically shown in Fig. 4a (see Methods), using the set-up of the Omicron VT-STM at room temperature (RT). As shown in Fig. 4b, the quantum wells (with a width of 6 nm here) were observed clearly by STM; that is, we could identify their location. In consideration of the energy levels in the quantum wells, we adjusted the photon energy to 1.51 eV (819 nm) for the 6 nm quantum well and 1.49 eV (834 nm) for the 8 nm quantum well, as shown in Fig. 4e.

The results are shown in Fig. 4c,d. In the quantum wells, the spin lifetimes were observed to be longer and increased with increasing well width, from 68 ± 6 ps ($(34 \pm 3) \times 2$ ps) for the 6 nm quantum well to 112 ± 6 ps ($(56 \pm 3) \times 2$ ps) for the 8 nm quantum well. According to the Dyakonov–Perel mechanism, the spin lifetime τ_s has a confinement-energy (E_{1e}) dependence of $\tau_s \approx E_{1e}^{-2}$ (see Methods). We estimated the confinement energy from the well widths, and the lifetimes are plotted as a function of the confinement energy in Fig. 4f. Macroscopically obtained results on multiple quantum wells are also shown for comparison[22]. According to Tackeuchi *et al.*[22], the lifetimes were different from sample to sample. Therefore, although it would be interesting to compare the results obtained for a single quantum well and multiple quantum wells, a discussion on the difference in lifetimes is left as

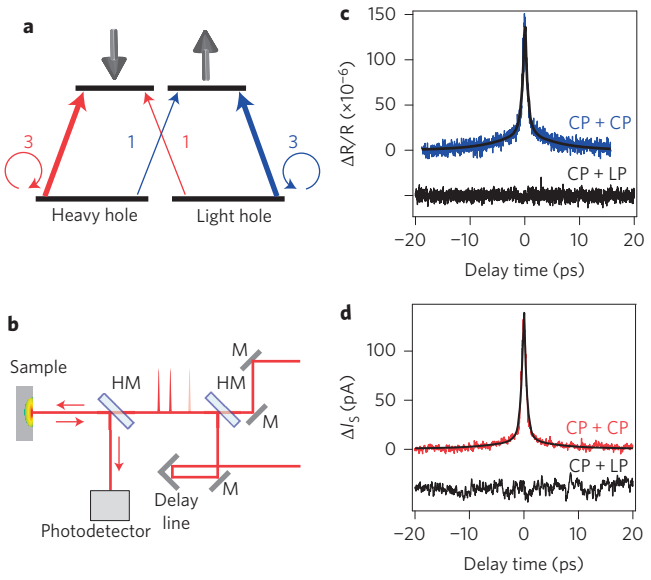

Figure 2 | OPP and OPP-STM measurements. a, Schematic diagram of transitions between heavy-hole/light-hole bands and $|\downarrow>$ and $|\uparrow>$ conduction band states, which indicate the relative transition strengths, 3:1 or 1:3, for light with R-rotation (red lines) or L-rotation (blue lines), respectively[2]. **b**, OPPR measurement set-up. The new modulation technique shown in Fig. 1 is used. **c**, OPPR spectrum with fitting curve (black line superimposed on blue signal). ΔR is the change in reflectivity. **d**, OPP-STM spectrum with fitting curve (black line superimposed on the red signal). ΔI_s is the change in spin-related tunnelling current (sample bias voltage $V_s = -0.9$ V, tunnelling current $I_t = 140$ nA, room temperature, laser intensity = 200 mW).

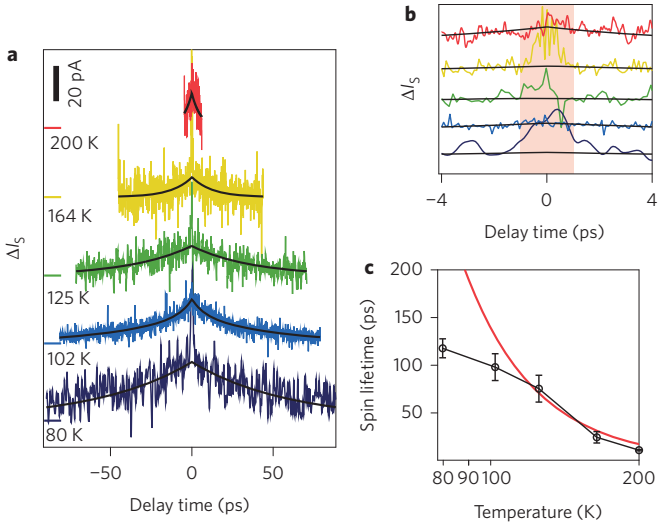

Figure 3 | Temperature dependence of spin dynamics in GaAs. **a**, Temperature-dependent OPP-STM spectra ($V_s = -1.0$ V, $I_t = 10$ nA, excitation wavelength = 813 nm, laser intensity = 200 mW). Black lines are fitting curves. The decay constants are 5.5±5.5 ps (200 K), 12±3 ps (164 K), 38±7 ps (125 K), 49±7 ps (102K) and 59±5 ps (80 K). **b**, Subsection of data in **a**. The intensity of the fast component decreased to close to the noise level at low temperatures, which is considered to be caused by the reduction of the excess energy because of the expansion of the bandgap. Thus, the fitting here was carried out after removing the central part shown by the coloured area in **b** (less than ±1.0 ps). We confirmed that the removal of further data above ±1.0 ps did not affect the lifetime obtained. **c**, Spin lifetime as a function of temperature. Data are shown by open circles with error bars of fitting in **a**. The solid red line represents the theoretical model, A^*T^{-3}, which has been validated by macroscopic experiments.

future work. The single-quantum well-level analysis of spin dynamics has become possible.

Figure 4g shows a cross-section of time-resolved signal across the 6 nm quantum well and the GaAs/AlGaAs interface obtained for $t_d = 2.3$ ps. As expected, the time-resolved signal rapidly increases (1) at the GaAs/AlGaAs interface and (2) at the interface between the AlGaAs layer and the quantum well. Both interfaces are adjacent to the AlGaAs region, in which no carriers are excited. A spatial resolution close to 1 nm has been achieved, which is considered to be limited, for example, by the signal-to-noise ratio.

As our final example, we demonstrate the results obtained by probing the quantum beat of spin precession in a magnetic field[2,23–25]. The Landé g factor for an electronic state in a semiconductor is highly sensitive to the characteristics of local electronic structures as well as to the associated band structures. Therefore, nanoscale evaluation of the g factor by OPP-STM is expected to provide a deeper analysis, enabling the fundamental understanding and theoretical modelling of quantum dynamics in materials and devices.

Measurements were carried out using an Omicron TESLA system, in which a uniform magnetic field of resolution better than 10^{-5} T can be applied to the sample below the STM tip over the scan area (here less than 1 μm × 1 μm). The experimental set-up is shown in Fig. 5a. An n-type GaAs sample with a donor concentration of 2×10^{16} cm^{-3}, which is near the value for a metal–insulator transition that provides a significantly long spin lifetime[26], was prepared by cleavage in a vacuum (2×10^{-8} Pa).

Figure 5b shows typical results for the magnetic-field dependence of spin precession obtained by OPP-STM at 2.5 K. In a magnetic field B, the precession of spins occurs at the Larmor frequency of $\omega = g\mu_B B/\hbar$, where g is the Landé g factor[27], μ_B is the Bohr magneton and $\hbar$ is the Dirac constant. The oscillation frequency of spin precession increases with increasing magnetic field. However, the oscillation in intensity, depending on the magnetic field, is caused by the repetition of laser pulses. Namely, when the repetition rate of the laser pulses, 11 ns (90 MHz), coincides with a multiple of the Larmor frequency, resonant amplification occurs[24,28]. This is the first successful probing of the precession dynamics of optically oriented spins by STM.

As shown in Fig. 5c, the signal (ΔI_S) consists of two components (ΔI_{S1} and ΔI_{S2}) with different spin lifetimes (τ_{S1} and τ_{S2}). Considering the lifetimes of the two components, S1 and S2 are, respectively, attributed to the spin relaxations of free conduction band electrons, which relax to delocalized donor-bound band electrons and delocalized donor-bound band electrons[25].

For S2, with a lifetime that appears to be longer than 11 ns, we carried out measurements of τ_{S2} using the resonant spin amplification (see Methods)[24,28]. Figure 5d shows the change in ΔI_S as a function of the magnetic field (red lines) and fitting curves (black lines). The upper blue line is the fitting error. Magnifications of some of the peaks in Fig. 5d are shown in Fig. 5e. For S1, τ_{S1} (<11 ns) was obtained by the fitting shown in Fig. 5c. The lifetimes of the two components, τ_{S1} and τ_{S2}, are shown in Fig. 5f. Further analysis by varying the measurement conditions, which was performed to a limited extent here, is necessary to understand the mechanism in detail.

Although there is a resonant amplification, the Larmor frequencies of S1 and S2 can be obtained accurately from the curves in Fig. 5b by the fitting shown in Fig. 5c because high-quality oscillations could be measured. Larmor frequencies are plotted as functions of magnetic field in Fig. 5g. The fitting

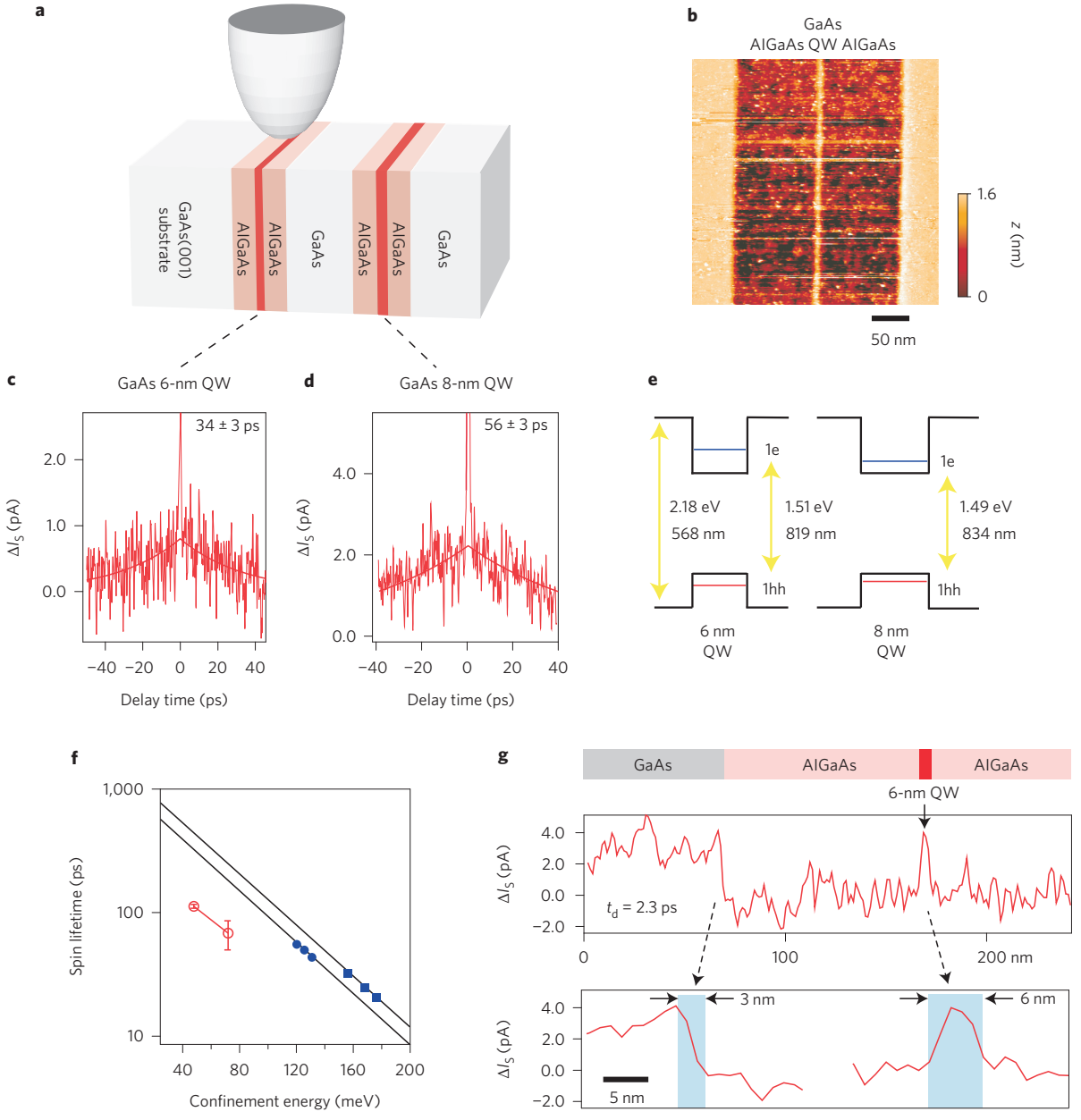

Figure 4 | OPP-STM measurement on quantum wells. a, Schematic structure of quantum wells with the STM tip. **b**, STM image of a quantum well ($V_s = 3.0$ V, $I_t = 100$ pA). **c**,**d**, OPP-STM spectra obtained for the 6-nm quantum well and the 8-nm quantum well, respectively ($V_s = -1.0$ V, $I_t = 8$ nA, laser intensity = 200 mW). Solid red lines are fitting curves. **e**, Band structure of quantum wells. 1e (blue lines) and 1hh (red lines) indicate the first excited states of electrons and heavy holes, respectively. Yellow arrows represent the AlGaAs bandgap energy and the 1e–1hh energies for the 6 nm quantum well and 8-nm quantum well. **f**, Confinement-energy dependence of the spin lifetime of carriers in a quantum well, with error bars of fitting in **c** and **d**. The two red circles with error bars represent the data. The results experimentally obtained by the OPPR method in Tackeuchi *et al.*[22] are also shown (blue dots on the two fitting black lines). **g**, Cross-sections of the time-resolved signal for $t_d = 2.3$ ps measured across the 6-nm quantum well and the GaAs/AlGaAs interface ($V_s = 4.0$ V, $I_t = 10$ nA, scan rate = 50 nm s^{-1}, time constant of lock-in = 10 ms). High bias voltages were used in **b** and **g** to enable measurement over the insulating AlGaAs area, in which no carriers are excited. Slight differences in measurement conditions are because of the adjustment for optimization, which depends on factors such as the tip and sample conditions in each case. However, the bias voltage and current did not have any discernible effect on the lifetime under our range of experimental conditions.

error of the Larmor frequency at each magnetic field was less than ±1%, which could not be shown on the graph. Therefore, the electron g factors deduced from the two slopes in Fig. 5g were −0.404 ± 0.002 and −0.435 ± 0.003 for S1 and S2, respectively. The deviation observed for S1 is attributed to the excess-energy dependence of the g factor for excited electrons[25,27]. We can now evaluate the electron g factor by STM through probing a spin-precession beat.

We have succeeded in developing an OPP-STM technique that enables the nanoscale probing of optically oriented spin dynamics with temporal resolution that corresponds to the optical pulse width. The combination of this technique with spin polarized (SP)-STM may enable further advancement of this field. We believe that this microscopy technique will make an important contribution to the further advancement of nanoscale science and technology.

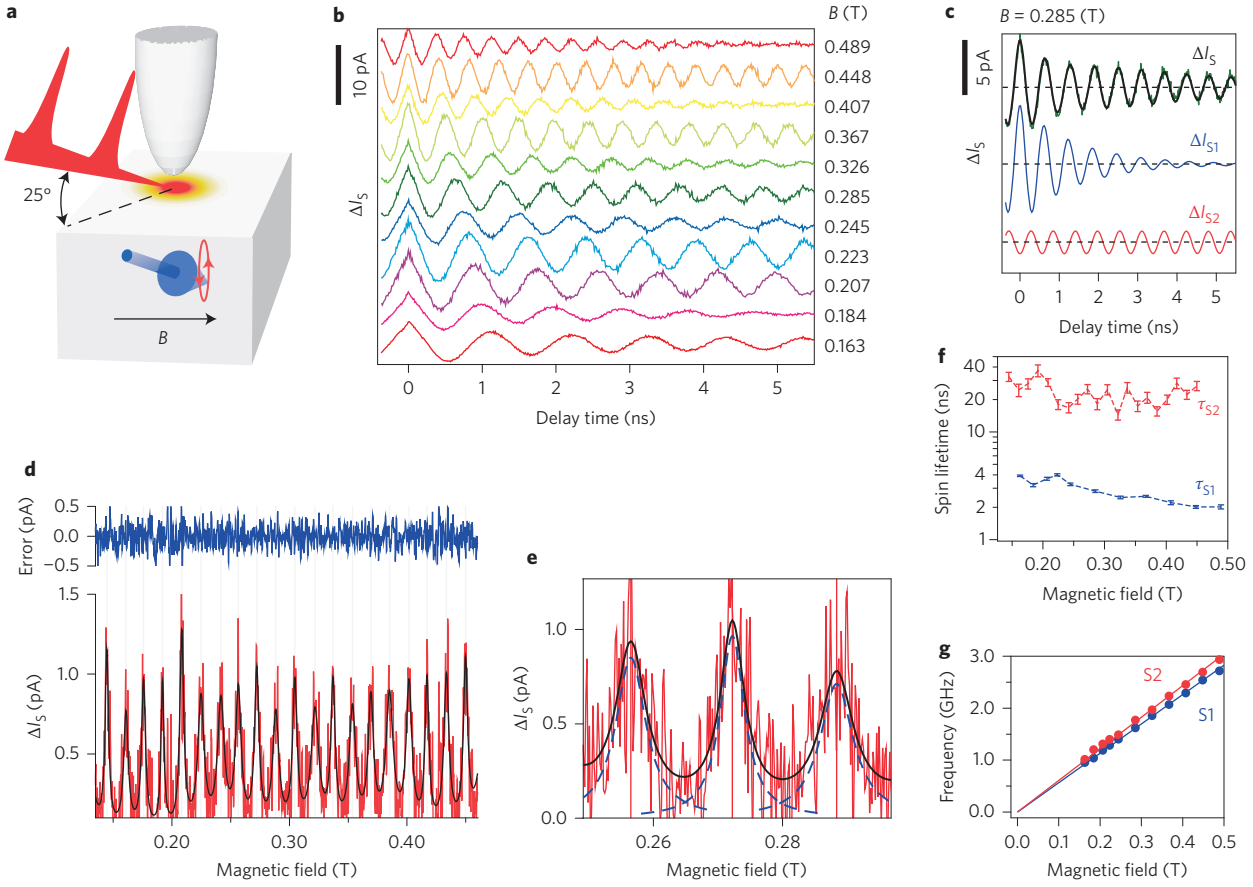

Figure 5 | Spin precession measurement by OPP-STM. a, Measurement geometry. Photoexcitation was carried out at an angle of 25° from the direction parallel to the sample surface. Blue and black arrows indicate spin and the externally applied magnetic field, respectively. The red spot below the STM tip represents the photoexcited area. **b**, Magnetic-field dependence of OPP-STM spectra ($V_s = 2.5$ V, $I_t = 3$ nA, excitation wavelength = 826 nm, laser intensity = 35 mW). **c**, Two components (blue and red lines) obtained by fitting the observed signal in **b** (green line) for the case of 0.285 T ($\Delta I_S = \Delta I_{S1} + \Delta I_{S2} = A_{S1}\exp(-t_d/\tau_{s1})\cos(\omega_{S1}t_d) + A_{S2}\exp(-t_d/\tau_{s2})\cos(\omega_{S2}t_d)$). The black line superimposed on ΔI_s (green line) is the fitting curve. **d**, ΔI_S as a function of magnetic field for $t_d = 1$ ps ($V_s = 1.5$ V, $I_t = 3$ nA). The black line superimposed on the data (red trace) is the fitting curve obtained by assuming the Lorentz curves, and its error is shown in the upper graph. The blue trace is the error between the data and the fitting. **e**, Magnification of some of the spectra in **d**. The black lines superimposed on the data (red trace) are the sums of Lorentz curves (blue dotted lines) fitted to the peaks (see Methods). **f**, Magnetic-field dependence of the spin lifetimes of the two components (shown with error bars of fitting). **g**, Precession frequencies $f = \omega/2\pi$ of the two components as a function of magnetic field, used to obtain the g factors. Solid lines are fitted lines assuming a linear relationship between ω and B, $\omega = g\mu_B B/\hbar$. The error bars are too small (less than 1%) to be shown.

Methods

Two titanium:sapphire lasers (Coherent, Chameleon 0.75 W and Mira 0.7 W, 90 MHz, duration ~130 fs) were used with the Synchrolock system (Coherent Inc) to produce pump and probe excitations. The circular polarizations of pump and probe laser pulses are modulated between L- and R-rotations at 1 MHz by controlling the directions of the LP light using Pockels cells (Fig. 1a). Each of the L- and R-rotation blocks has 90 laser pulses, and the delay time between pump and probe pulses is indicated by $t_d = t_{d1}$ in the top diagram in Fig. 1b.

As the signal is very weak, a lock-in detection method is necessary, in which modulating the excitation without inducing thermal expansion is the key factor[11]. When polarization is modulated, even a slight difference in light intensity between L- and R-polarizations is critical, and the introduction of a new modulation method is essential.

When a 1 kHz difference is given between the pump and probe modulation frequencies, for example, 1.001 MHz for the pump pulse and 1 MHz for the probe pulse, the relative phase of the two circular polarizations changes at 1 kHz, as shown in Fig. 1b, where the delay time between pump and probe pulses is fixed at a certain value t_{d1}. The difference in frequencies, 1 kHz in this case, is used as the reference frequency for the lock-in detection method. Accordingly, the co-CP and counter-CP excitations are mixed and their ratio changes at 1 kHz, as shown in Fig. 1c. With this method, the influence of the polarization-dependent change in light intensity, which may be introduced unintentionally, can be removed.

The number of electrons excited by the co-CP ($n_{ex}^{co}(t_d)$) and counter-CP ($n_{ex}^{count}(t_d)$) excitations provide the two points for a delay time t_{d1}, as shown by the two circles on the signal lines in Fig. 1d, and is reflected in the signal tunnelling current $I_s(t_d)$. Therefore, when the delay time is changed simultaneously with the modulation of circular polarizations described here, the OPP-STM signal provides a difference of ΔI_s, that is, the difference between the two signal lines obtained by the co-CP and counter-CP excitations. Here the delay time was changed by the Synchrolock system used for the synchronization of the pump and probe pulses. The jitter of the Synchrolock system we used was 200 fs at best, which reduces the temporal resolution in the subpicosecond range in this case. A system with better resolution using a laser with a shorter pulse and reduced jitter is necessary for the detailed analysis of the fast component.

The sample of GaAs/$Al_{0.3}Ga_{0.7}$As quantum wells was grown on a GaAs(100) (undoped) substrate and two quantum wells with widths of 6 nm and 8 nm were formed, as shown in Fig. 4a. A 200 nm GaAs layer was placed as a spacer to isolate the two quantum wells to reduce the effect of the relative interaction between them. We cleaved the sample to produce a clean (110) surface, similarly to the first example. In the quantum wells, the energy levels of the upper bands (heavy- and light-hole bands) shown in Fig. 2a split owing to the strain caused by the lattice mismatch between GaAs and AlGaAs layers[29]. Therefore, we can excite fully polarized spins, which makes the measurements easier because the signal becomes stronger[17]. According to the Dyakonov–Perel mechanism, the spin lifetime in a quantum well can be expressed as $\tau_s \approx (k_B T)^{-1} E_{1e}^{-2}$, $E_{1e} = n^2h^2/(8ma^2)$, $n = 1$, where k_B is the Boltzmann constant, h is the Planck constant, m is the electron mass, a is the lattice constant, and E_{1e} is the confinement energy for $n = 1$ (ref. 22).

Spectra were analysed basically using a function that consists of two exponential components and a constant corresponding to the offset caused by the slight

difference in the intensities between the right-handed and left-handed lights and the slight deviation from circular polarization (see the caption to Fig. 3 for the other spectral analysis procedure shown in Figs 3a,b). All spectra were drawn with the horizontal axis adjusted to compensate for the offset.

In the case of a spin lifetime longer than the laser repetition rate, the lifetime can be obtained using resonant spin amplification[24,28]. As shown in Fig. 5d, the carrier spin has sharp resonances as a function of the magnetic field. Here the spectra were fitted by the sum of the Lorentz curves (dotted lines in Fig. 5e), as shown by the black solid lines in Fig. 5d,e. The value of τ_{S2} for each peak was obtained from the full-width at half-maximum of each Lorentz curve.

Received 22 December 2013; accepted 22 May 2014; published online 29 June 2014

References

1. Zutic, I., Fabian, J. & Sarma, S. D. Spintronics: fundamentals and application. *Rev. Mod. Phys.* **76,** 323–410 (2004).
2. Dyakonov, M. I. *Spin Physics in Semiconductors* (Springer Series in Solid-State Sciences 157, Springer, 2008).
3. Wiesendanger, R. Spin mapping at the nanoscale and atomic scale. *Rev. Mod. Phys.* **81,** 1495–1550 (2009).
4. Loth, S., Etzkorn, M., Lutz, C. P., Eigler, D. M. & Heinrich, A. J. Measurement of fast electron spin relaxation times with atomic resolution, A. J. *Science* **329,** 1628–1630 (2010).
5. Khajetoorians, A. *et al.* Current-driven spin dynamics of artificially constructed quantum magnet. *Science* **339,** 55–59 (2013).
6. Kemiktarak, U., Ndukum, T., Schwab, K. C. & Ekinci, K. L. Radio-frequency scanning tunnelling microscopy. *Nature* **450,** 85–89 (2007).
7. Mamin, H. J., Birk, H., Wimmer, P. & Rugar, D. High speed scanning tunneling microscopy: principles and applications, *J. Appl. Phys.* **75,** 161–168 (1994).
8. Kodera, N., Yamamoto, D., Ishikawa, R. & Ando, T. Video imaging of walking myosin V by high-speed atomic force microscopy. *Nature* **468,** 72–76 (2010).
9. Terada, Y, Yoshida, S., Takeuchi, O. & Shigekawa, H. Laser-combined scanning tunneling microscopy for probing ultrafast transient dynamics. *J. Phys. Condens. Matter.* **32,** 264008–264015 (2010).
10. Hamers, R. J. & Cahill, D. G. Ultrafast time resolution in scanned probe microscopies. *Appl. Phys. Lett.* **57,** 2031–2033 (1990).
11. Grafström, S. Photoassisted scanning tunneling microscopy. *J. Appl. Phys.* **91,** 1717–1753 (2002).
12. Cocker, T. L. *et al.* An ultrafast terahertz scanning tunnelling microscope. *Nature Photon.* **7,** 620–625 (2013).
13. Terada, Y., Yoshida, S., Takeuchi, O & Shigekawa, H. Real-space imaging of transient carrier dynamics by nanoscale pump–probe microscopy. *Nature Photon.* **4,** 869–974 (2010).
14. Yokota, M. *et al.* Bases for time-resolved probing of transient carrier dynamics by optical pump–probe scanning tunneling microscopy. *Nanoscale* **5,** 9170–9175 (2013).
15. Yoshida, S. *et al.* Single-atomic-level probe of transient carrier dynamics by laser-combined scanning tunneling microscopy *Appl. Phys. Express* **6,** 032401 (2013).
16. Kirilyuk, A., Kimel, A. V. & Rasing, T. Ultrafast optical manipulation of magnetic order. *Rev. Mod. Phys.* **82,** 2731–2784 (2010).
17. Tackeuchi, A., Muto, S., Inata, T. & Fujii, T. Direct observation of picosecond spin relaxation of excitons in GaAs/AIGaAs quantum wells using spin-dependent optical nonlinearity. *Appl. Phys. Lett.* **56,** 2213–2215 (1990).
18. Hohenester, U. *et al.* Subpicosecond thermalization and relaxation of highly photoexcited electrons and holes in intrinsic and p-type GaAs and InP. *Phys. Rev. B* **47,** 13233–13245 (1993).
19. Kimel, A. V. *et al.* Room-temperature ultrafast carrier and spin dynamics in GaAs probed by the photoinduced magneto-optical Kerr effect. *Phys. Rev. B* **63,** 235201–235208 (2001).
20. Bungay, A. R., Popov, S. V., Shatwell, I. R. & Zheludev, N. I. Direct measurement of carrier spin relaxation times in opaque solids using the specular inverse Faraday effect. *Phys. Lett. A* **234,** 379–383 (1997).
21. Zerrouati, K., Fabre, F., Bacquet, G., Bandet, J. & Frandon, J. Spin-lattice relaxation in p-type gallium arsenide single crystals. *Phys. Rev. B* **37,** 1334–1341 (1988).
22. Tackeuchi, A., Kuroda, T., Muto, S. & Wada, O. Picosecond electron-spin relaxation in GaAs/AlGaAs quantum wells and InGaAs/InP quantum wells. *Physica B* **272,** 318–323 (1999).
23. Lai, T. *et al.* Evolution of spin coherence dynamics and *g* factor with electron excess energy in bulk intrinsic GaAs. *Appl. Phys. Lett.* **91,** 062110 (2007).
24. Kikkawa, J. M. & Awschalom, D. D. Resonant spin amplification in n-type GaAs. *Phys. Rev. Lett.* **80,** 4313–4316 (1998).
25. Schreiber, L., Heidkamp, M., Rohleder, T., Beschoten, B. & Güntherodt, G. Mapping of spin lifetimes to electronic states in n-type GaAs near the metal–insulator transition. Preprint at http://arxiv.org/:0706.1884 (2007).
26. Dzhioev, R. I. *et al.* Low-temperature spin relaxation in n-type GaAs. *Phys. Rev. B* **66,** 245204 (2002).
27. Oestreich, M. *et al.* Temperature and density dependence of the electron Landé *g* factor in semiconductors. *Phys. Rev. B* **53,** 7911–7916 (1996).
28. Yugova, I. A., Glazov, M. M., Yakovley, D. R., Sokolova, A. A. & Bayer, M. Coherent spin dynamics of electrons and holes in semiconductor quantum wells and quantum dots under periodical optical excitation: resonant spin amplification versus spin mode locking. *Phys. Rev. B* **85,** 125304 (2012).
29. Davies, J. H. The *Physics of Low-dimensional Semiconductors: An Introduction* (Cambridge Univ. Press, 2006).

Acknowledgements

Support from Japan Society for the Promotion of Science (Grants-in-Aid for Scientific Research, 22226003) is acknowledged.

Author contributions

S.Y. performed the experiment and data analysis (with H.S.). Y.A., Z.W. and Y.M. assisted with the measurement. R.O. and H.O. worked on sample preparation. E.M. helped to design the TESLA system. O.T. provided technical advice and helped to design the TESLA system. H.S. organized and supervised the project and edited the paper.

Additional information

Reprints and permissions information is available online at www.nature.com/reprints. Correspondence and requests for materials should be addressed to H.S.

Competing financial interests

The authors declare no competing financial interests.